Structure of the ATP Synthase Complex (ECF_1F_0) of *Escherichia coli* from Cryoelectron Microscopy†

Uwe Lücken,‡ Edward P. Gogol, and Roderick A. Capaldi*
Institute of Molecular Biology, University of Oregon, Eugene, Oregon 97403
Received October 25, 1989; Revised Manuscript Received February 22, 1990

ABSTRACT: The structural relationship of the catalytic portion (ECF_1) of the *Escherichia coli* F_1F_0 ATP synthase (ECF_1F_0) to the intact, membrane-bound complex has been determined by cryoelectron microscopy and image analysis of single, unordered particles. ECF_1F_0, reconstituted into membrane structures, has been preserved and examined in its native state in a layer of amorphous ice. Side views of the ECF_1F_0 show the same elongated bilobed and trilobed projection of the ECF_1 views shown previously to be normal to the hexagonal projection [Gogol, E. P., Lücken, U., Bork, T., & Capaldi, R. A. (1989) *Biochemistry 28*, 4709–4716]. The elongated aqueous cavity of the ECF_1 is perpendicular to the membrane bilayer profile in the bilobed view. ECF_1 is separated from the membrane-embedded F_0 by a narrow stalk ~40 Å long and ~25–30 Å thick. The F_0 part extends from the lipid bilayer by ~10 Å on the side facing the ECF_1. There is no clear extension of the protein on the opposite side of the membrane.

F_1F_0-type ATPases are multisubunit enzyme assemblies which couple transmembrane proton gradients to ATP synthesis and hydrolysis. They are comprised of two separate subassemblies, a catalytic domain extrinsic to the bilayer, the F_1, and a membrane-embedded proton channel, the F_0. In *Escherichia coli*, the F_1 part is made up of five different subunits, α, β, γ, δ, and ϵ, in a stoichiometry of 3:3:1:1:1, and contains three catalytic sites, one on each β subunit. The F_0 part contains three subunits (a, b, and c) in the *E. coli* enzyme and provides the proton channel, involving subunits c and a. This channel is blocked by reaction of dicyclohexylcarbodiimide (DCCD) with a buried carboxyl of the c subunit [reviewed in Pedersen et al. (1981), Sebald and Hoppe (1981), Vignais and Lunardi (1985), and Senior (1988)].

We have recently determined the structure of ECF_1 at low (~25-Å) resolution by electron microscopy (Gogol et al., 1989a,b). The α and β subunits are elongated masses arranged hexagonally around a central cavity with their long axes at right angles to the hexagonal projection. They are interdigitated for most of the length of the molecule. There is a seventh mass, most probably comprised of part of the γ subunit, located at one end of the structure, partly occluding the internal cavity.

An understanding of the orientation of F_1 with respect to F_0 is essential for assessing proposed mechanisms of ATP hydrolysis and synthesis. Schematic representations of F_1F_0 have generally shown F_1 on membranes with the hexagonal projection as the top view (Fillingame, 1981; Pederson et al., 1981; Aris & Simoni, 1983; Senior, 1988), although there is no experimental verification of this orientation. Recently, Tsuprun et al. (1989) have visualized the hexagonal projection as well as other orientations of the F_1, in negatively stained membranes viewed edge-on.

To clarify the orientation of F_1 on F_0, we have extended our studies on ECF_1F_0 using cryoelectron microscopy of specimens embedded in a thin layer of amorphous ice (Gogol et al., 1987). We have collected many more side views of the enzyme than used in our preliminary analysis and compared these views with images of ECF_1. The data indicate that ECF_1 is oriented with its pseudohexagonal axis projection normal to the plane of the membrane.

Materials and Methods

Preparation and Reconstitution of ECF_1F_0. ECF_1F_0 was prepared and reconstituted into membrane structures at a high protein-to-lipid ratio as described previously (Aggeler et al., 1987).

Reconstitution of ECF_1F_0 into vesicles with a low protein-to-lipid ratio was accomplished by mixing 500 μL of ECF_1F_0 (0.5 mg/mL), containing 0.35 mg/mL egg phosphotidylcholine (Sigma), 0.75% deoxycholate, and 1.25% potassium cholate, with 200 μL of egg phosphatidylcholine (10 mg/mL) dissolved in 4% potassium cholate, under a nitrogen atmosphere. The mixture was sonicated briefly with a Branson sonifier equipped with a microtip and then stirred for 1 h at 4 °C. The clear solution was dialyzed at 4 °C against two changes of 100 mL of 50 mM Tris-HCl (pH 7.5), 5 mM $MgSO_4$, 1 mM DTE, and 20% glycerol over 2 days, followed by an additional day of dialysis against 100 mL of 20 mM 3-(*N*-morpholino)-propanesulfonic acid (MOPS, pH 7.5), 50 mM KCl, 0.5 mM EDTA, and 10% glycerol. The vesicles were pelleted by ultracentrifugation at 144000*g* for 45 min and resuspended in the MOPS–KCl buffer.

ATPase assays were performed in the ATP regenerating assay mixture of Lötscher et al. (1984), using ~2 μg of ECF_1 or ~5 μg of ECF_1F_0, or specimens frozen in amorphous ice on electron microscope grids coated with holey carbon films. Samples were tested for lauryldimethylamine oxide (LDAO) activation by addition of 50 μL of 10% LDAO (Fluka) into 1 mL of assay mixture. DCCD sensitivity was assayed by preincubation with 10 μM DCCD in the above buffer for 1 h at room temperature; inhibition was relieved (95–100%) by LDAO addition, as described, to demonstrate that the DCCD effect was F_0-mediated.

Electron Microscopy and Image Analysis. Specimens for cryoelectron microscopy were prepared as described by Gogol et al. (1989a) using samples with protein concentrations of ~1 mg/mL. Micrographs were recorded as described (Gogol

† This work was funded by NIH Grants HL24526 and GM39806 to R.A.C. and by NATO Training Fellowship 300-402-5036 from the DAAD to U.L. Microscopy facilities were funded by NIH Grant RR02756 and computer facilities by a grant from the Lucille P. Markey Foundation.

‡ Present address: Frizt-Haber Institute of the Max Planck Society, Department of Electron Microscopy, Faradayweg 4-6, D-1000 Berlin 33, Federal Republic of Germany.

0006-2960/90/0429-5339$02.50/0 © 1990 American Chemical Society

et al., 1989a), at a magnification of 57000× and a defocus of 1 μm with an estimated electron dose of ~20 e/A^2.

Areas of micrographs were selected and digitized by using a scan step size of 25 μm, corresponding to 4.4 Å at the specimen. Images were displayed on a raster graphics terminal, and 64 × 64 pixel areas (282 × 282 Å), approximately centered on particles, were windowed by using the SPIDER image analysis program (Frank et al., 1981). The images were scaled to the same average density and internal variance, yielding approximately the same range of values for each particle. Each image was circularly masked to reduce surrounding background noise and Fourier low-pass-filtered at a resolution of 20 Å to remove high-frequency noise. The images were then aligned by using autocorrelation and cross-correlation procedures, first to a single clear image and then iteratively to averages of 10 aligned images. Misaligned images were easily identified by the poor positioning of their gross features (bilayer and F_1), as well as relatively low correlation to the reference image. Averages were calculated by adding corresponding pixels and then rescaling the resulting image.

Three different strategies were employed to sort the F_1F_0 images into classes of similar views: visual inspection, correlation fit to selected images, and correspondence analysis. A preliminary examination of the filtered images revealed three common motifs in the F_1 portion, each represented in a substantial fraction of the particles, though with variable clarity. For a correlation-based classification of the data set, the five clearest and most representative images from each visually identified category were averaged to create reference images. Correlation coefficients were calculated (with SPIDER option CC) between each reference and individual image, masking out all but a circular area including the F_1 portions of the molecules. Images were assigned to the class with the highest correlation coefficient.

For correspondence analysis, each image was interpolated down to 24 × 24 pixels (11.7 Å/pixel) to reduce the information content and statistical fluctuations within the images, and masked to include only the F_1 portion. Analysis was performed by using the SPIDER program, and factor maps were examined to determine clustering and separation of images into categories.

Results

Enzyme Preparation and Intactness of the Complex under Conditions for Electron Microscopy. ECF_1F_0 was reconstituted with phospholipid into membranes over a range of protein-to-lipid ratios, producing ribbons, sheets, and vesicles containing the enzyme complex. Thin films of these suspensions were formed under conditions which minimized evaporation (4 °C, high humidity); these films were immediately rapidly frozen to embed the specimens in a layer of amorphous ice, and maintained in this state during electron microscopy.

The ECF_1F_0 complex is unlikely to be denatured when rapidly "frozen" in physiological buffers, but it could be dissociated into ECF_1 and F_0 by the treatment, a possibility that was examined by assaying the activity of enzyme which had been frozen on holey carbon grids, as described under Materials and Methods. Figure 1 shows that ATPase activity of ECF_1F_0 is retained under rapid freezing conditions and there is the same activation by the detergent LDAO (i.e., ~4-fold) as obtained with enzyme which had not been subjected to the treatment. The critical result, shown in Figure 1, is the DCCD inhibition of the enzyme preparation. ECF_1F_0 was 95% inhibited by addition of 10 μM DCCD, a value similar to that of control preparations. DCCD inhibits the ATPase activity

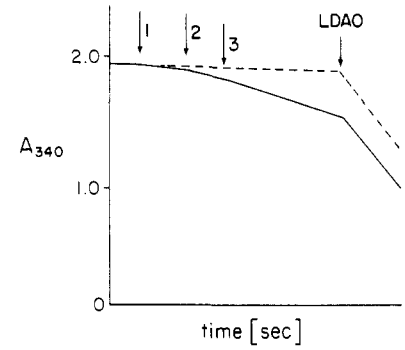

FIGURE 1: ATPase activity of ECF_1F_0 frozen on electron microscope grids. Decrease in absorbance indicates ATPase activity. At times indicated by arrows labeled 1, 2, and 3, single electron microscope grids were added to the reaction mixture. At the time indicated by the labeled arrow, LDAO was added to a concentration of 0.5% to stimulate ATPase activity. Solid line, native ECF_1F_0. Dashed line, ECF_1F_0 treated with DCCD prior to application and freezing. As shown by the dashed line, ATPase activity is inhibited by DCCD; the inhibition is released by addition of LDAO.

of the ECF_1F_0 by binding to subunit c of the F_0 (Sebald & Hoppe, 1981); this inhibition therefore establishes the integrity of the ECF_1F_0 preparation under the conditions used for cryoelectron microscopy.

Examination of the ECF_1F_0 Complex in Different Views. Typical electron micrographs of ribbons (A) and sheets (B) and vesicles (C and D) incorporating ECF_1F_0 are shown in Figure 2. "Top" views of the enzyme complex (normal to the vesicle surface) could be found in the center of vesicle preparations, but these showed little resemblance to any of the views of ECF_1 alone described earlier. This is not surprising as top views of ECF_1F_0 in vesicles are a projection through ECF_1 (90 Å), the stalk (45 Å), F_0 (60 Å), and a second lipid bilayer from the other side of the vesicle (50–60 Å). It is not predictable how the features of these different components would superimpose, so an analysis of top views was not attempted.

The orientation of ECF_1F_0 can still be determined by examination of the side views of the membrane-embedded enzyme, provided these images can be related to views of ECF_1. Individual molecules are readily identified at the edges of vesicles and edge views of ribbons (Figure 2). These images were chosen for further analysis; the criteria for image selection were lack of obvious overlap with neighboring molecules and clear visibility of the membrane bilayer profile.

These side views were iteratively aligned, first using a single well-defined image of high contrast as reference and then using an average of 10 such aligned images of ECF_1F_0. A total of 170 of the 223 initially selected images appeared to align properly to the reference image; the average of these 170 images is shown in Figure 3A.

The average of all 170 images is expected to include views through the molecule from all directions around its circumference, and thus is a cylindrical projection of the ECF_1F_0. Visual inspection of the images provisionally identified three types of F_1 projections represented in substantial numbers: one with two vertical lobes of density, separated by a vertical cleft; one with three approximately vertical lobes, separated, though less clearly, by two clefts; and a more even distribution of density, with a centered cavity. A subjective classification placed approximately 65% of the particles into these 3 categories, distributed as 57 vertically bilobed, 25 trilobed, and 29 "centered". The remaining images which did not appear to belong in any of these classes were usually less distinctly defined, and did not appear to share common features.

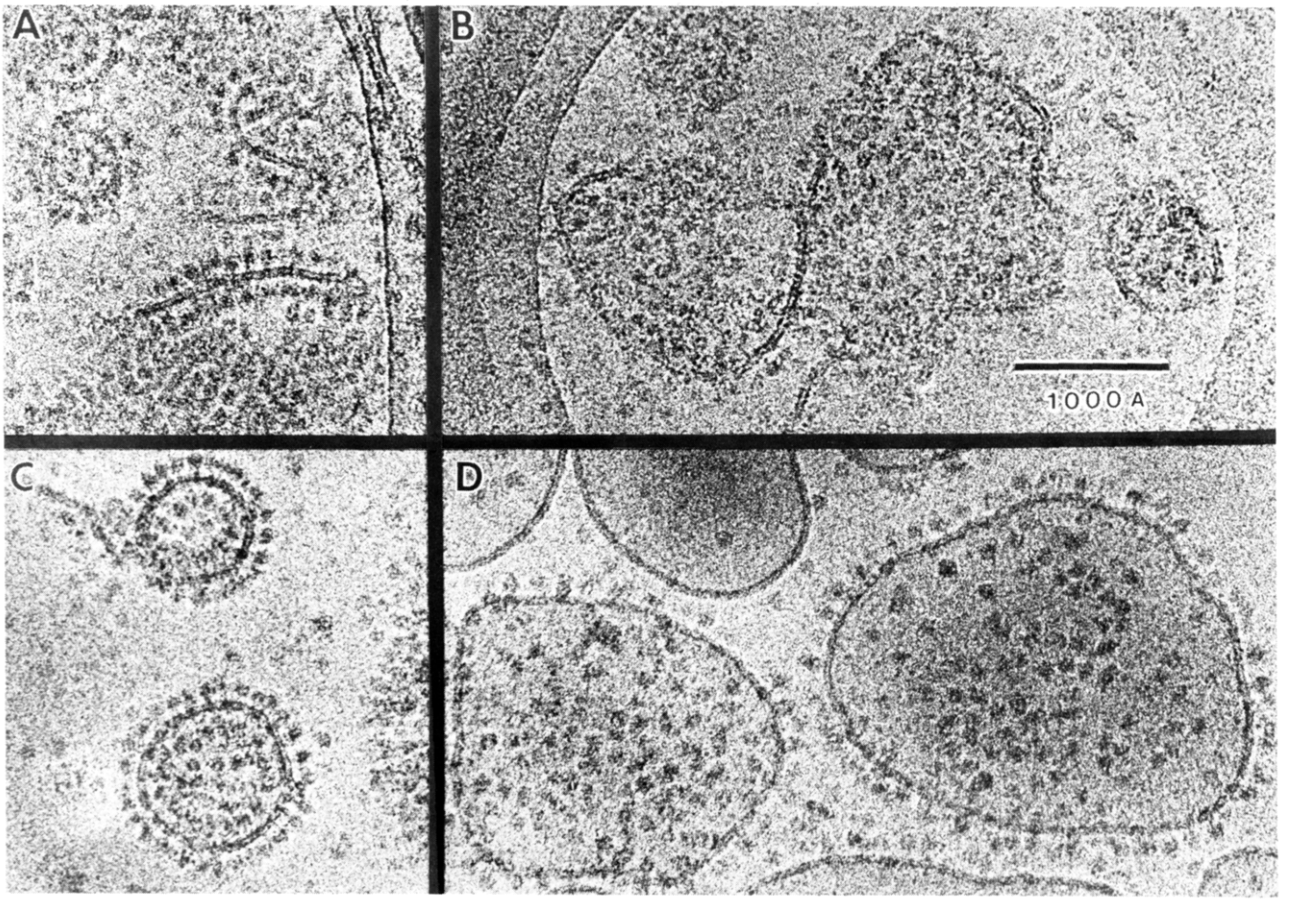

FIGURE 2: Cryoelectron micrographs of reconstituted ECF_1F_0 preparations. (A, B, C) Narrow ribbons (viewed edge-on), sheets, and vesicles of F_1F_0 at a protein-to-lipid weight ratio of approximately 1. (D) Vesicles formed at a higher lipid-to-protein ratio (approximately 10:1).

A more objective analysis was effected by creating reference images, based on the clearest and most extreme examples of the above categories, and calculating correlation coefficients between each reference and each image. Since poorly defined particles do not contribute to (and may detract from) the clarity of the resulting averaged images, 25% of the particles were eliminated from consideration, based on their low correlation coefficient to the references (or to the global average). Of the remaining images, 48 correlated best to a bilobed reference, 31 to a trilobed reference, and 49 to one with a central cavity. The averages obtained by this classification are shown in Figure 3B–D.

Correspondence analysis was attempted to test the validity of this classification. This procedure defines two-dimensional functions (eigenfactors) which describe the variation of major features among all the images in a data set (Bretaudiere & Frank, 1986). By examining the distribution of values of the eigenfactors among the images, the images may be grouped into self-consistent clusters. The ECF_1F_0 data failed to produce clear divisions in eigenfactor maps, so it was not possible to uniquely define classes. A nonclustered distribution is expected for continually variable data, as may be anticipated for the projection angles of ECF_1F_0 side views. One pair of eigenfactors (the first and the fourth, in order of size) allowed a segregation of the images into three categories, representing the three classes described above. Since the distribution of the images was nearly continuous, the positioning of the separating curves was guided by the results of the correlation-based classification. Including all the images in the analysis, 67 were included in the bilobed category, 26 in the trilobed, and 74 in the central cavity. Agreement with the image classification by correlation coefficients was 66%. Averages of the images thus sorted (not shown) did not deviate significantly from those in Figure 3B–D, save for some degeneration of features, probably due to inclusion of images of marginal quality.

Structural Features of the ECF_1 Part of the Complex. The outline of the ECF_1 is similar in all four averaged ECF_1F_0 projections shown in Figure 3. In each case, this structure is $\simeq$90 Å in its vertical dimension and 85–90 Å side at its center, but clearly tapered (to 60–70-Å diameter) at the end further from the bilayer. This tapered appearance is an important clue to the orientation of ECF_1 on F_0. Figure 4A shows the shape of ECF_1 based on our structural analysis of two-dimensional crystals of this part of the ATP synthase (Gogol et al., 1989a). The molecule is symmetric in the hexagonal (top) projection (not shown) but shows a characteristic tapered appearance in side view.

The internal features of the individual classes of views also indicate that the side views of ECF_1F_0 are projections normal to the pseudohexagonal axis of ECF_1. One class of ECF_1F_0 exhibits a bilobed appearance in the ECF_1, and another a trilobed view. Similar views of ECF_1 have previously been described and deduced to be side views of ECF_1 [cf. Figures 3B with 4B and 3C with 4C). Both the bilobed and trilobed projections of ECF_1F_0 have the aqueous cavity (inside the ECF_1 part) perpendicular to the plane of the membrane. The contrast of the vertical clefts is lower in the ECF_1F_0 images than in the ECF_1 images, but this is partly due to the greater total projection density in these thicker specimens; i.e., a thicker layer of ice is necessary to embed the membranous structures. (Contrast enhancement in the display to make the clefts more prominent results in loss of other features such as the stalk connecting the ECF_1 with the F_0.)

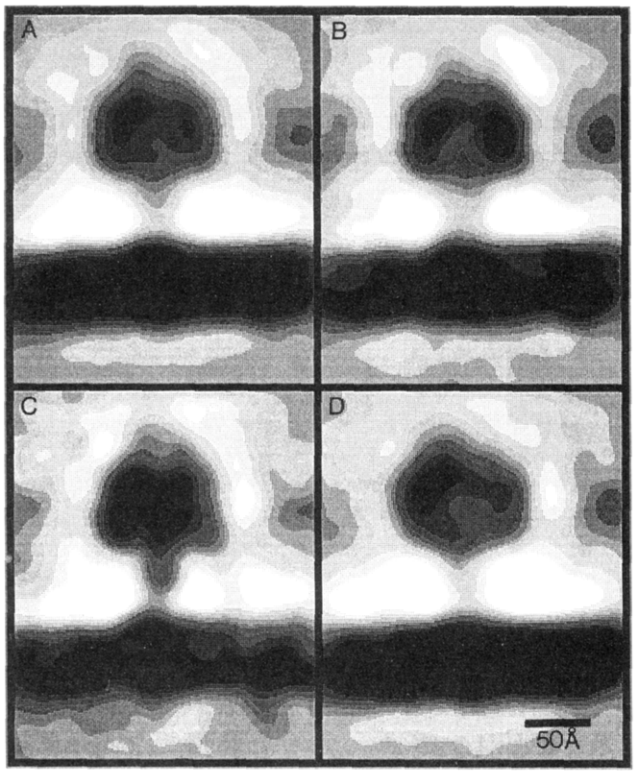

FIGURE 3: Averaged images of side views of ECF_1F_0. (A) Average including all 170 images selected, aligned, and screened as described. Averages based on correlation coefficient analysis. (B) 48 images classified as vertically bilobed. (C) 31 images classified as vertically trilobed. (D) 49 images which contained low density at their centers, but without a clear vertical groove.

The third class of images of the ECF_1F_0, likewise selected by the appearance of the ECF_1 and representing ~29% of the particles, appears to have a more central aqueous cavity, reminiscent of the hexagonal view of the enzyme (Figure 3D). However, the overall shape of the molecule in the projection is clearly asymmetric, and the surrounding density is bilobed rather than hexagonally modulated. This may be a view down the cleft of the ECF_1 part in an orientation which superimposes the small subunits (γ, δ, and ϵ), that are believed to be at the interface between the ECF_1 part and the stalk, on the cleft.

Features of the Stalk. The overall average and each of the classified averages of the ECF_1F_0 (Figures 3) clearly show the presence of a stalk connecting the ECF_1 to the membrane-embedded F_0. This structure is ~40 Å long and is consistently 25–30 Å wide in each of the side views, even though two of the three classes of projections of the ECF_1 are different viewing directions. This consistent width indicates that the stalk is a relatively cylindrical structure.

Features of the F_0 Part. The F_0 part of the complex is less distinct than the other parts of the ATP synthase. There is a small protrusion from the membrane on the side facing the ECF_1, while the opposite side of the bilayer appears to be flat. Most of the F_0 part thus appears to be confined to the 50-Å width of the lipid bilayer.

Discussion

Our studies of ECF_1F_0 are the first application of cryoelectron microscopy to the study of a membrane protein using single-particle analysis (Gogol et al., 1987). We have used this approach, along with the more conventional electron microscopy in negative stain, to determine the low-resolution three-dimensional structure of ECF_1 (Gogol et al., 1989a). The work described here examines the membrane-bound ECF_1F_0 complex. Features of the F_1 part are revealed, along with the structural feature linking the catalytic part to the protein-translocating F_0.

Cryoelectron microscopy is particularly useful for examining ECF_1F_0, as the complex is potentially unstable under conditions of conventional negative staining, with phosphotungstic acid stripping many ECF_1 particles from membranous preparations (Racker et al., 1969; Gogol et al., 1989a). Here we have demonstrated by activity assay that ECF_1F_0 is preserved as an intact complex in amorphous ice.

We have previously described the low-resolution structure of ECF_1; this shows the α and β subunits hexagonally arranged as roughly cylindrical structures, clearly interdigitated for approximately 60 Å. At one end, the molecule becomes tapered (from ~90-Å diameter at the center to 65 Å) and appears to show 3-fold symmetry instead of the hexagonal outline of the rest of the structure. The opposite end is not as drastically tapered (~80-Å diameter), but more circular with no clear modulations. For much of their length, the α and β subunits surround a central cavity (Gogol et al., 1989a,b). An additional protein density probably made up of the γ subunit, and possibly parts of the other small subunits, is asymmetrically located toward one end of this cavity.

The results presented here orient ECF_1 with respect to the membrane bilayer and in relation to the F_0 part of the entire ATP synthase complex. Side views of ECF_1F_0 in vesicles and ribbon structures all have a consistent outline of the ECF_1, tapered at the end away from the membrane. Half of all of the molecules examined display bilobed or trilobed projections of their ECF_1 portions, similar to those previously described for isolated ECF_1. These projections are interpreted as views normal to the pseudohexagonal axis of the ECF_1. Differences between these side projections of free and F_0-bound ECF_1 are partially due to the higher contrast possible with molecules not associated with membranes. Subunit rearrangements are also expected to occur during binding of ECF_1 to F_0, to form the connecting stalk, and perhaps internally in the F_1 to couple enzymatic activity to proton flow. These anticipated structural changes are evidently small enough to preserve the essential feature of "side" views of ECF_1.

Very few of the 170 images of ECF_1F_0 examined had any hexagonal features, like those which predominate in fields of ECF_1 molecules examined in negative stain (Akey et al., 1983; Boekema et al., 1988), and which are common (20–30% of particles) in fields of ECF_1 molecules embedded in ice (Gogol et al., 1989a). One class of ECF_1F_0 images has a circular and centrally located low-density region, rather than the single or double clefts of low density seen in bilobed and trilobed projections, respectively. However, like the other two classes of views, this projection of the ECF_1 is tapered at the end away from the bilayer and is bilobed rather than hexagonally modulated at the periphery. It may represent a side view of ECF_1 in which the small subunits (that are most likely located at the junction with the stalk) fall into a particular line of sight through the ECF_1F_0. Similar views were not readily identified in fields of ECF_1, either due to their low numbers or because of a rearrangement of the small subunits in ECF_1 dissociated from membrane.

Approximately 35% of all of the particles examined did not correspond to any of the main projections. These included some potentially overlapping images, more noisy data, and molecules in previously unrecognized views. These were not hexagonal views when examined individually, or when averaged to reduce the noise inherent to the images (result not shown).

We conclude, therefore, that ECF_1F_0 is oriented in the

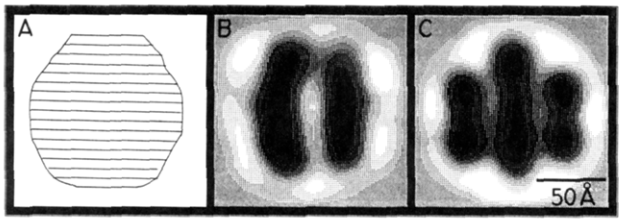

FIGURE 4: Side views of ECF_1, from the analysis of Gogol et al. (1989a). (A) Outline of the three-dimensional structure embedded in negative stain. Projections from cryoelectron microscope images: (B) bilobed view (63 images); (C) trilobed view (56 images).

membrane with the pseudohexagonal axis of ECF_1 normal to the bilayer. This arrangement of the enzyme is in agreement with the conclusions of Tsuprun et al. (1989), which are based on examination of individual images of negatively stained specimens of mammalian F_1F_0. The data presented by Tsuprun et al. are a collection of single-molecule images which include both hexagonal and more nondescript views. As the authors themselves point out, adsorption to the carbon substrate and drying membrane-bound complexes in negative stain may induce some reorientation of the particles, possibly about their weakest points, resulting in a nonnative orientation of the F_1 domains. Examination of F_1F_0 in amorphously frozen, unsupported films eliminates this source of distortion.

The more comprehensive analysis of images of ECF_1F_0 in this study than in our previous work (Gogol et al., 1987) adds more information about the features of the stalk and F_0 part of the ATP synthase complex. The link between ECF_1 and F_0 is a stalk whose dimensions are consistent among all of the averaged side view images. Since the bilobed and trilobed subclasses are views of the molecule from different directions, the constant dimension indicates that the stalk is roughly cylindrical with a diameter of 25–30 Å. A structure of this sort could be constructed by close-packing of six or seven α-helices. Biochemical analysis suggests that the stalk includes parts of the two b subunits of F_0, each contributing two α-helices in hairpin arrangements (Perlin et al., 1983; Hermolin et al., 1983; Senior, 1983; Schneider & Altendorf, 1984). Other subunits implicated in the interaction between ECF_1 and F_0 are the δ, γ, and α subunits (Futai et al., 1974; Sternweis & Smith, 1977; Bragg & Hou, 1975; Dunn et al., 1980; Aggeler et al., 1987; Gavilanes-Ruiz et al., 1988).

The F_0 part of ECF_1F_0 is poorly defined in the side view averages. Most of the mass of this part of the complex is within the bilayer. There is a small protrusion of the structure on the same side of the membrane as the ECF_1 part, but essentially no density extending from the other side of the membrane. A compact and mostly bilayer-embedded structure might be anticipated from topological studies of the F_0 subunits. The predicted folding pattern of subunit a is six or seven transmembrane helices, with very little protein outside the bilayer (Walker et al., 1984; Cox et al., 1984). Subunit b has been shown to span the membrane in a single pass, possibly an α-helix, with a short amino-terminal hydrophilic stretch on one side of the bilayer (opposite from the ECF_1) and the long carboxy-terminal hydrophilic sequence in the stalk region (Walker et al., 1984; Hoppe & Sebald, 1984; Schneider & Altendorf, 1987). Finally, subunit c has been found to span the membrane as a hairpin structure with a hydrophilic loop on the ECF_1 side of the membrane, and only very short hydrophilic sequences extending from the other side of the bilayer (Hoppe & Sebald, 1984; Schneider & Altendorf, 1987).

The dimensions of the ECF_1F_0 complex in the membrane obtained in our study differ from those reported for the F_1F_0 complex of chloroplasts examined as detergent-embedded aggregates. We find a maximum dimension of F_0 accross the membrane of 60 Å compared with a value of 80 Å for CF_0 obtained by Boekema et al. (1988). This may be due to the difference in composition between CF_0 and the F_0 part of the *E. coli* ATP synthase.

ACKNOWLEDGMENTS

We thank Trisha Ryan and Barbara Robbins for preparation of the ECF_1F_0 used in this work.

REFERENCES

Aggeler, R., Zhang, Y.-Z., & Capaldi, R. A. (1987) *Biochemistry 26*, 7107–7113.
Akey, C. W., Crepeau, R. H., Dunn, S. D., McCarty, R. E., & Edelstein, S. J. (1983) *EMBO J. 2*, 1409–1415.
Aris, J. P., & Simoni, R. D. (1983) *J. Biol. Chem. 258*, 14599–14609.
Boekema, E. J., van Heel, M., & Gräber, P. (1988) *Biochim. Biophys. Acta 933*, 365–371.
Bragg, P. D., & Hou, C. (1975) *Arch. Biochem. Biophys. 167*, 311–321.
Bretaudiere, J.-P., & Frank, J. (1986) *J. Microscopy 144*, 1–14.
Cox, G. B., Jans, D. A., Fimmel, A. L., Gibson, F., & Hatch, L. (1984) *Biochim. Biophys. Acta 768*, 201–208.
Dunn, S. D., Heppel, L. A., & Fullmer, C. S. (1980) *J. Biol. Chem. 255*, 6891–6896.
Fillingame, R. H. (1981) *Curr. Top. Bioenerg. 11*, 35–106.
Frank, J., Shimkin, B., & Dowse, H. (1981) *Ultramicroscopy 6*, 343–358.
Futai, M., Sternweis, P. C., & Heppel, L. A. (1974) *Proc. Natl. Acad. Sci. U.S.A. 71*, 2725–2729.
Gavilanes-Ruiz, M., Tommasino, M., & Capaldi, R. A. (1988) *Biochemistry 27*, 603–609.
Gogol, E. P., Lücken, U., & Capaldi, R. A. (1987) *FEBS Lett. 219*, 274–278.
Gogol, E. P., Lücken, U., Bork, T., & Capaldi, R. A. (1989a) *Biochemistry 28*, 4709–4716.
Gogol, E. P., Aggeler, R., Sagermann, H., & Capaldi, R. A. (1989b) *Biochemistry 28*, 4717–4724.
Hermolin, J., Gallant, J., & Fillingame, R. H. (1983) *J. Biol. Chem. 258*, 14550–14555.
Hoppe, J., & Sebald, W. (1984) *Biochim. Biophys. Acta 768*, 1–27.
Lötscher, H. R., deJong, C., & Capaldi, R. A. (1984) *Biochemistry 23*, 4140–4143.
Pedersen, P. L., Schwerzmann, K., & Cintron, N. (1981) *Curr. Top. Bioenerg. 12*, 149–199.
Perlin, D. S., Cox, D. N., & Senior, A. E. (1983) *J. Biol. Chem. 258*, 9793–9800.
Racker, E., Horstmann, L. L., Kling, D., & Fessenden-Raden, J. M. (1969) *J. Biol. Chem. 244*, 6668–6674.
Schneider, E., & Altendorf, K. (1985) *EMBO J. 4*, 515–520.
Schneider, E., & Altendorf, K. (1987) *Microbiol. Rev. 51*, 477–497.
Sebald, W., & Hoppe, J. (1981) *Curr. Top. Bioenerg. 12*, 1–64.
Senior, A. E. (1983) *Biochim. Biophys. Acta 726*, 81–95.
Senior, A. E. (1988) *Physiol. Rev. 68*, 177–231.
Sternweis, P. C., & Smith, J. B. (1977) *Biochemistry 16*, 4020–4025.
Tsuprun, V. L., Orlova, E. V., & Mesyanzhinova (1989) *FEBS Lett. 244*, 279–282.
Vignais, P. V., & Lunardi, J. (1985) *Annu. Rev. Biochem. 54*, 977–1014.
Walker, J. E., Saraste, M., & Gay, N. (1984) *Biochim. Biophys. Acta 768*, 164–200.